Proceedings of the Canadian Society for Mechanical Engineering International Congress 2022
CSME Congress 2022
June 5-8, 2022, Edmonton, AB, Canada

Numerical investigation of hydrodynamic forces acting on a flexible pitching filament

Aysan Gholami[1], Behrooz Afra[2], Ali Tarokh[1,2,3]
[1]Environmental Engineering, Lakehead University, Thunder Bay, Canada
[2]Faculty of Science and Environmental Studies, Lakehead University, Thunder Bay, Canada
[3]Department of Mechanical Engineering, Thunder Bay, Canada

Abstract— This study investigates the pitching motion of an elastic filament flapping in a uniform laminar flow. The Lattice Boltzmann Method (LBM) as the fluid solver and the Lattice Spring Model (LSM) as the solid structure solver are employed to solve filament motion in the flow. The LBM and LSM are both mesoscopic models based on the kinetic theory. However, their emergent behavior captures the continuum properties of the system. The boundary force effects on the near fluid nodes are calculated using Immersed Boundary Method (IBM). The mutual behavior of the flow and deformable filament has been examined in a channel to understand the role of flexibility, oscillation frequency, and pitching amplitude on lift and drag coefficients. It can be inferred from the results that the lift coefficient (C_L) is mainly affected by pitching amplitude (θ_0), and its fluctuation amplitude showed significant values while θ_0 equals 3° and 5°. In contrast, changing the frequency has a negligible effect on C_L. Moreover, the drag coefficient (C_D) increases with the frequency until it reaches the maximum amount at 0.13; afterward, it decreases sharply. In addition, lower pitching amplitude causes a higher C_D. Considering the rigidity effects, the results revealed that increasing rigidity does not always coincide with a reduction in the filament's ending fluctuation. The filament's end tends to have an increase in oscillation amplitude when the non-dimensional rigidity number exceeds 0.01.

Keywords: Flexible filament, pitching motion, fluid-structure interaction, immersed boundary method, lattice Boltzmann method

I. INTRODUCTION

The last few years have seen an increased interest in studying the behavior of filaments as an abstraction for modeling physical phenomena like flag flapping and bio-locomotion [1-6]. Filaments, due to their slender and flexible structure, can be a prototype for understanding different phenomena like swimming and flapping motions ranging from whales to insects [7]. For instance anguilliform swimmers' style, categorized as undulatory motion, can be modeled by filaments due to their elongated fairly uniform body [8]. So based on their complex structure and motion type only a specific range of oscillation frequencies are meaningful [9]. The mutual interaction of a flexible solid structure with the surrounded fluid is challenging due to their free motion and complex geometries. Numerical modeling gives insight into the interplay between the solid and fluid-structure to investigate their collaborative effects [4]. So far, LBM has proved to be a reliable method, especially dealing with complex geometries. It solves the problems in the mesoscopic scale and is considered to be a bottom-to-up methodology that employs the discrete Boltzmann equation to reach macroscopic properties. In addition, the existence of a solid structure (especially elastic solid) inside the fluid flow domain needs a closer and distinct treatment that is known as the Fluid-Structure Interaction problem. In this respect, LSM is proved to be a promising approach capable of tracking solid interaction with the environment and its deformation due to exerted forces. It consists arrangement of invariant Hookean springs in a lattice with specific stiffness to describe the flexibility and deformation of the solid. Moreover, fast grid-regeneration of the LSM has emerged a new interest in coupling them together in different fields of studies [10, 11]. This model can be directly mapped onto linear elasticity theory through the correct choice of spring constants.

A significant number of researches have been conducted on contributive parameters on the filament's motion. Yuan et al.[12] and Li et al. [2] studied the flexibility effects of filaments with different lengths and mass ratios using IBM carried out on the particles in a viscous flow. Gerivani and Nazari [13] employed the IB-LBM along with lattice Spring Damper Model on viscoelastic filaments in which it is capable of predicting elastic filaments either. The effects of mass ratio and filament's length on oscillation patterns have been studied thoroughly. Tian et al. [4] exerted the IB-LBM to predict fish movement in entrainment and Karman gait regions. They attempt to model single and multiple filaments in a uniform flow. The separation distance, geometrical properties of the filament, and Strouhal number of the shedding flow behind a rigid cylinder were analyzed thoroughly for both regions. Within this area of investigation, a number of investigations have been devoted to studying drag and lift effects on the hydrodynamic forces acting on the body.

The focus of the works in this paper is on the influential parameters, frequency, and pitching amplitude, on the lift and drag coefficients. Although the filament motion can be a combination of heaving and pitching motions, only the pitching motion is considered in this study. Pitching motion is responsible for the most percentage of the thrust forces. So, it is worth considering how big is its effects on the lift, drag coefficients.

Moreover, in order to have an insight into flexibility influence on the free end of the filament, different rigidities magnitudes have been investigated.

II. NUMERICAL MODEL AND METHODOLOGY

A. *LBM for the fluid domain*

The LBM tracks the fluid behavior via the assembly of particles using the distribution function f_i at position $\vec{r}$ and time t. It consists of two processes: collision and streaming. The LBM equation with external force is given as below:

$$\underbrace{f_i(\vec{r}+\vec{e}_i\Delta t, t+\Delta t)-f_i(\vec{r},t)}_{streaming}=\underbrace{\tau^{-1}\left[f_i(\vec{r},t)-f_i^{eq}(\vec{r},t)\right]}_{collision}+\underbrace{F(\vec{r},t)}_{force} \quad (1)$$

here, $\vec{e}_i$ is the lattice speed that streams the particles with the time intervals of Δt to the neighbor node. The collision step is characterized by the non-dimensional relaxation time that is related to viscosity, $\nu = c_s^{\,2}(\tau - \frac{1}{2})$ where $c_s^{\,2}$ is the speed of sound; it embraces all the evolutions that happen to the distribution function. f_i^{eq} is the equilibrium state of the density distribution function, which is described as:

$$f_i^{eq}(\vec{r},t) = w_i\rho\left[1+\frac{3}{c^2}(\vec{e}_i.\vec{u})+\frac{9}{2c^4}(\vec{e}_i.\vec{u})^2-\frac{3}{2c^2}\vec{u}.\vec{u}\right]. \quad (2)$$

The D2Q9 lattice structure is employed that is accompanied by w_i weight coefficient, *u* local velocity, and ρ density.

Exerting the external force in the simulation field may vary based on the method that is trained. Here, the discrete-forcing method proposed by Guo et al. [14] is considered:

$$F_i(\vec{r},t) = (1-\frac{1}{2\tau})w_i\left[3\frac{\vec{e}_i-\vec{u}(\vec{r},t)}{c^2}+9\frac{\vec{e}_i.\vec{u}(\vec{r},t)}{c^4}\right].F(\vec{r},t) \quad (3)$$

here, $(\vec{r})$ represents Lagrangian point position and $F_i(\vec{r},t)$ Lagrangian Elastic force density due to the deformation of the structure. The force is accompanied in the simulation field in two stages, momentum exchange at time $t+\frac{dt}{2}$ as $\frac{\delta t}{2}F(\vec{r},t)$ and after the collision at $t+dt$ as $F_i(\vec{r},t)$.

B. *Immersed Boundary Method (IBM)*

Objects immersed and fluid have an interaction with each other. This interaction affects the fluid covering the boundary and the deformation of the boundary in an elastic structure. This phenomenon is obviously observable in aquatic locomotion, red blood cells moving in the vein (Cardiac fluid dynamic) [11], and engineering structures. In order to impose a no-slip boundary condition on the solid boundary, the promising IBM has been employed. The basic idea is to approximate a boundary by a set of off-lattice marker points that affect the fluid only *via* a force field. In other words, IBM is employed to tackle the forces that each phase imposes on the other. It leads to the necessity of an interpolation stencil to couple the lattice and the marker points that can be set either diffusely or sharply [15]. The whole scenario is described by Eulerian and Lagrangian systems mathematically. The Eulerian system is represented by a fixed, regular grid *(x,t)* on which the fluid lives, and the Lagrangian system is an ensemble of marker points ($\vec{r}_i$) to describe material properties of the solid [16]. Due to the displacement of the

The forces describe the fluid-structure interaction equations on the boundary nodes that are indicated as:

$$F(\vec{r}_b, t+\delta t) = \rho\frac{\vec{U}_b - \vec{u}_b(\vec{r}_{\,b}, t+\delta t)}{\delta t/2} \quad (4)$$

where $\vec{U}_b$ and $\vec{u}_b$ are the velocity on the boundary points and non-forced velocity that is:

$$\vec{u}_b = \sum_{b=1}^{n}\vec{u}(\vec{r}_{ij},t)D(\vec{r}_{ij}-\vec{r}_b). \quad (5)$$

So the external force on the interface can be imposed as:

$$F(\vec{r},t) = \sum_{b=1}^{n}\vec{F}(\vec{r}_b,t+\delta t)D(\vec{r}_{ij}-\vec{r}_b)\Delta S_b \quad (6)$$

ΔS_b is the arc length of boundary division and $D(\vec{r}_{ij}-\vec{r}_b)$ is the Dirac's delta function as the critical ingredient for IBM, which is expressed as:

$$D(\vec{r}_{ij}-\vec{r}_b) = \frac{1}{h^2}d(\frac{x_{ij}-x_b}{h})d(\frac{y_{ij}-y_b}{h}) \quad (7)$$

Function *d(r)* is:

$$d(r) = \begin{cases} \frac{1}{8}(3-2|\vec{r}|)+\sqrt{1+4|\vec{r}|-4|\vec{r}|^2} & 0\le|\vec{r}|<1 \\ \frac{1}{8}(5-2|\vec{r}|)+\sqrt{-7+12|\vec{r}|-4|\vec{r}|^2} & 1\le|\vec{r}|<2 \\ 0 & |\vec{r}|\ge 2 \end{cases} \quad (8)$$

Since they are different systems, to couple them together, the information between these two systems should be transferred via velocity interpolation and force spreading.

C. *LSM for the solid structure*

In the LSM, the particles of a solid structure are connected to each other through linear invariant springs. To acquire higher accuracy, the spring constants, type of lattice, and the mass of particles should be selected carefully. The isentropic springs' mechanical behavior is described by Youngs Modulus *E* and Poisson's ratio ν that assign quantities of $\nu = \frac{1}{3}$ and $E = \frac{8k_n}{3}$

in the simulation. k_n is the normal springs stiffness that can be related to the diagonal spring stiffness k_{n-n} as $k_n = \frac{k_{n-n}}{2}$. In this study, a square spring arrangement is employed, in which each massless spring is connected to four straight and four diagonal springs [17]. It has been proved that the macroscopic properties of the filament can be converted into spring stiffness using arguments from standard continuum mechanics [18].

By calculating the $\vec{r}_{ij}$, relative position vector between neighbor nodes *i* and *j*, the forces associated with deformation of each lattice point can be considered as:

$$\vec{F}_{ij}^{spring} = \sum_{i=1}^{4} -k_n \Delta\vec{r}_{ij} + \sum_{i=1}^{5} -k_{n-n} \Delta\vec{r}_{ij}. \quad (\vec{r}_{ij} = \vec{r}_i - \vec{r}_j) \tag{9}$$

III. COMPUTATIONAL MODEL

For bodies placed parallel to upstream, understanding the forces acting on the interface has paramount importance. Although the flow may remain uniform, the flow near the fluid-body interface may be unsteady and cause displacement of the body. In the case of filaments, due to their slender structure, their motion can be a combination of heaving and pitching movement. The former one refers to the linear motion along the vertical axis, and the latter is defined as the angular motion that can be described as:

$$\theta(t) = \theta_0 \cos(2\pi ft + \varphi). \tag{10}$$

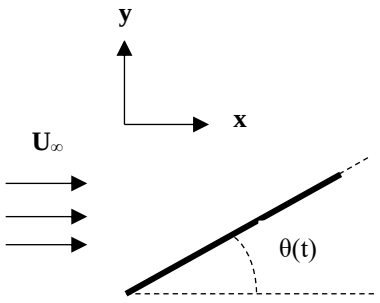

Figure 1. A schematic of pure pitching motion.

As shown in Fig. 1, θ_0 is the pitching amplitudes of the leading edge. The oscillation frequency and phase offset of the motions is contributed as *f and* φ in the equation, respectively. The non-dimensional pitching frequency can be tracked by Strouhal number ($St = \frac{fL}{U_\infty}$) as an important parameter, in which *L* is the characteristic length and U_∞ the uniform inlet velocity.

A robust hybrid model is needed to be presented to explore the link between the fluid-structure interaction of an elastic filament. In this regard, the LBM for the fluid domain and LSM for solid deformation are combined together. In addition, to investigate boundary interactions IB-LBM as an advantageous approach in simulation of moving boundaries have been employed [19]. In order to investigate the effects of pitching amplitude and Strouhal number on drag and lift coefficients, the simulation of a flexible filament with the length of L=40 and width of 5 has been carried out (see Fig. 2). It is placed in the center of the channel. Other crucial parameters' magnitude is mentioned in Table 1. Not included in Table 1. are the uniform inlet velocity that equals 0.05 and Reynolds number equals 300. It is worth mentioning that all the units are described in lattice units.

Table 1. Physical parameters used in the simulation.

St	θ_0	*Ca*
0.005-0.27 (interval: 0.01)	3-15 (interval: 2)	0.001, 0.005, 0.01, 0.1, 0.55, and 1

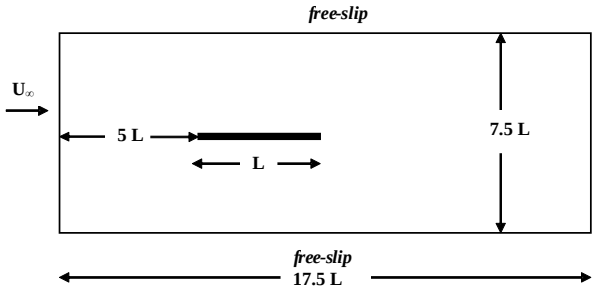

Figure 2. The schematic of the filament and the channel.

To ensure free-slip boundary condition on the lower and upper surface of the channel, a non-equilibrium bounce-back condition is applied [20]. Also, uniform velocity for inlet and outflow boundary conditions are considered. The corners at the inlet and outlet points are treated carefully. In order to investigate flexibility effects on the filament fluctuations, Capillary number is introduced as:

$$Ca = \frac{EI}{\rho U_\infty^2 L^3} \tag{11}$$

It represents the ratio of elasticity forces to the viscosity effects where E, I and ρ are elasticity, moment of inertia and density of the filament, respectively.

Based on the forces calculated on the boundaries, drag and lift coefficient can be defined as:

$$C_D = \frac{F_x}{\frac{1}{2}\rho U_\infty{}^2 L} \tag{12}$$

$$C_L = \frac{F_y}{\frac{1}{2}\rho U_\infty{}^2 L} \tag{13}$$

In which F_x and F_y are horizontal and vertical fluid forces generated on the surface.

IV. RESULTS

The mean value of C_D and C_L in each cycle based on the Strouhal number and pitching amplitude variations are shown in Fig.3a and Fig.3b. There is a slight and subtle difference in mean values of C_L across *St* variation. However, it mainly affects C_D where a peak point is revealed at *St*=0.13. For lower *St*, the drag increases until it reaches the maximum amount that is because of viscosity effects on the surface and high deformation pattern that can be interpreted as fluid forces domination on the filament. Increasing hydrodynamic forces over filament not only causes higher oscillation amplitude and deformation, but also it is compatible with the increase of C_D. As shown in Fig. 4, the flapping takes place at lower *St* with a higher rate, which leads to higher C_D. The results agree with the findings in [8, 13].

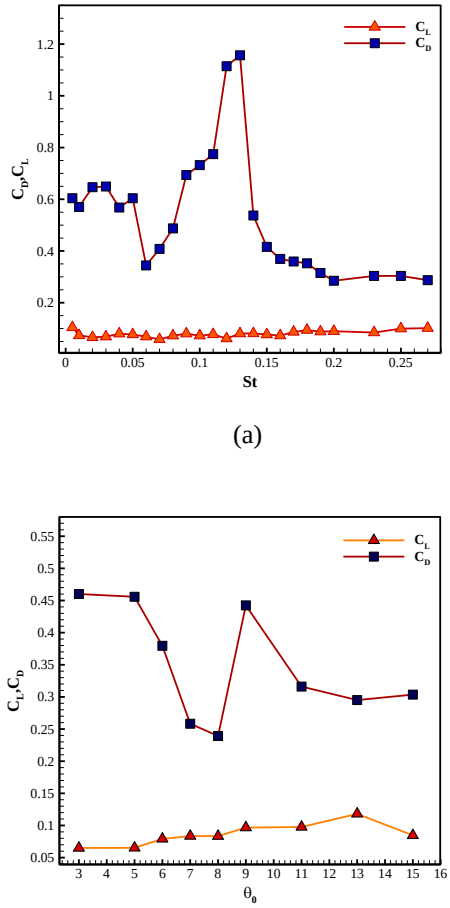

Figure 3.The variation of drag and lift coefficients as function of a) Strouhal number and b) pitching amplitude for *Ca*=0.01.

It can be inferred from Fig. 3b that θ_0 impose the same effects as does the St on C_D. This can be interpreted as the fact that increasing θ_0 results in a reduction of instantaneous pitching amplitude (Eq. 10) during the flapping cycle [21]. Contrary to C_D, C_L reveals insignificant dependency to *St*. However, with higher pitching amplitude, C_L increases subsequently.

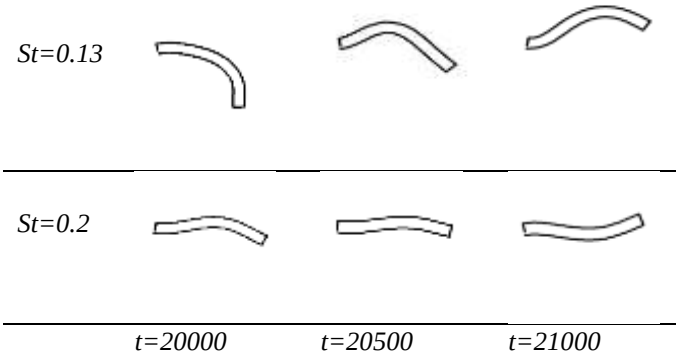

Figure 4. The filament deformation at *St*=0.13 and 0.2 for three sequential time steps at *Ca*=0.01.

Fig.5 shows the oscillation amplitude of different pitching amplitudes. As it is evident lower pitching amounts (especially θ_0=3,5), oscillation represents greater amplitude changes. However, the mean C_L in Fig. 3b it is almost close to zero.

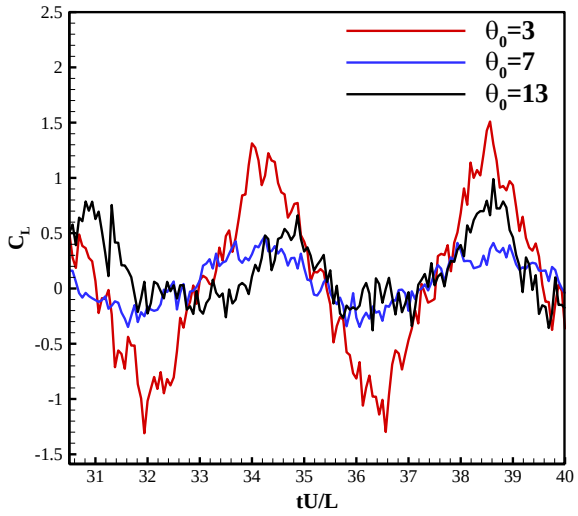

Figure 5. The time history of C_D for θ_0=3,7,13.

It is reasonable to accept that the more rigid (higher *Ca*) is the filament, the lower is the filament's end motion. However, as shown in Fig. 6, increasing the rigidity of the filament (higher *Ca*) does not always result in lower ending displacement. For $Ca > 0.01$, although the filament tends to a more rigid state, the distance between the two ends of the filament increases. Also, the amplitude of the oscillation pattern decreases, which leads to a narrower displacement. It can be related to the natural frequency of the flapping motion that creates resonant. Similar results have been found in [17].

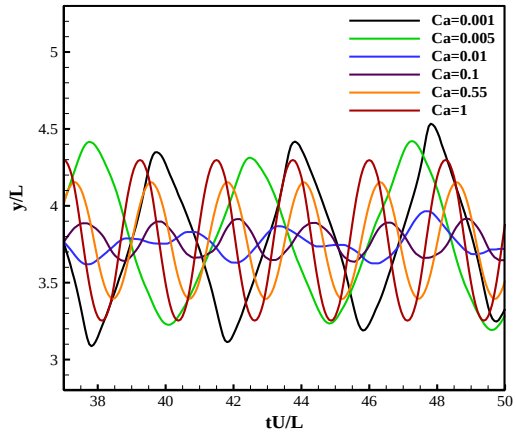

Figure 6. The time evolution of filament's ending motion for different rigidities.

Fig. 7 depicts the instantaneous streamwise velocity contour at three different instant time steps. The control parameters for this case are: *Ca*=0.01, *St*=0.01, and θ_0=15˚. As shown in the figure, the vortices are prone to increase and lose their coherence by the passing of time. The shed vertices become more significant, and their number increases at *t=55*. The flapping characteristics expand the velocity vector in the *x*-direction and bending region of the filament. At the bending point, the velocity increases.

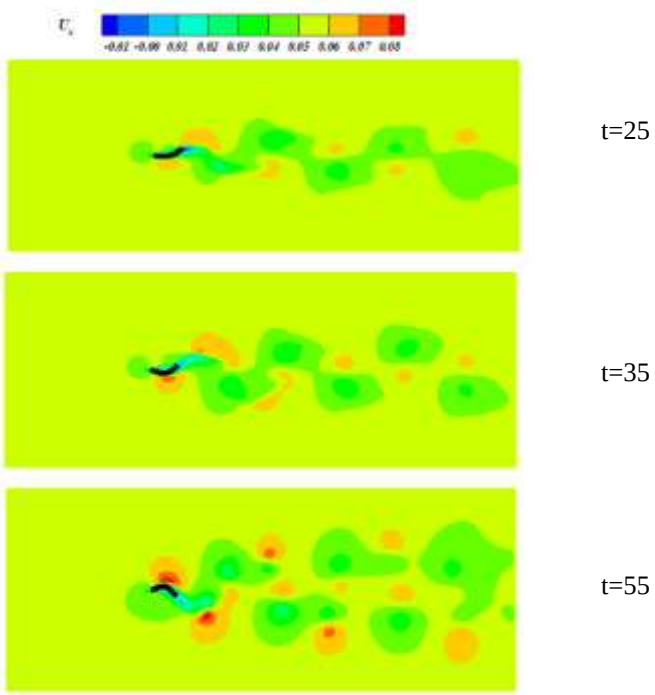

Figure 7. The x-components velocities contour of fluid around flexible filament at t=25,35,55.

That is, the fluid exerts force to push the filament to its previous state. When the structure moves and deforms there is going to be a deformation force pushing the structure back to its preferred position and the geometry changing of deformable body results in a time-dependent effect on the local flow. Likewise, when the fluid is moving, the structure moves as same fluid velocity local to all the structure points.

V. CONCLUSION

This study used IB-LBM combined with LSM to analyze the effects of Strouhal number and pitching amplitude on lift and drag coefficients over a flexible filament flapping at Reynolds number of 300 for a specific range of parameters. C_L shows subtle sensitivity to the St variation; however, by increasing θ_0, it tends to augment sensibly. On the other hand, C_D maintains an incremental trend with St until it reaches a peak at $St = 0.13$ and decreases sharply afterwards. That can be described because of a higher rate of deformation. θ_0 imposes almost the same effect on C_D that is lower θ_0 causes higher C_D and by an increase in its magnitude C_D increases too. Moreover, the role of flexibility on the free end of the filament is studied. The ending motion magnitude is reduced by increasing rigidity until it reaches $Ca = 0.01$; afterward, the oscillation increases with higher amplitude. A closer look at the x-component velocity contour at St=0.01 shows that by increasing, the flapping of the filament velocity on the bending point increases. It is because of the fluid forces that impose the filament to its previous condition.

REFERENCES

[1] G. Eason, B. Noble, and I. N. Sneddon, "On certain integrals of Lipschitz-Hankel type involving products of Bessel functions," Phil. Trans. Roy. Soc. London, vol. A247, pp. 529–551, April 1955. *(references)*

[2] J. Clerk Maxwell, A Treatise on Electricity and Magnetism, 3rd ed., vol. 2. Oxford: Clarendon, 1892, pp.68–73.

[3] I. S. Jacobs and C. P. Bean, "Fine particles, thin films and exchange anisotropy," in Magnetism, vol. III, G. T. Rado and H. Suhl, Eds. New York: Academic, 1963, pp. 271–350.

[4] K. Elissa, "Title of paper if known," unpublished.

[5] R. Nicole, "Title of paper with only first word capitalized," J. Name Stand. Abbrev., in press.

[6] Y. Yorozu, M. Hirano, K. Oka, and Y. Tagawa, "Electron spectroscopy studies on magneto-optical media and plastic substrate interface," IEEE Transl. J. Magn. Japan, vol. 2, pp. 740–741, August 1987 [Digests 9th Annual Conf. Magnetics Japan, p. 301, 1982].

[7] Kim, W. and H. Choi, *Immersed boundary methods for fluid-structure interaction: A review*. International.

[8] Afra, B., et al., Direct numerical simulation of freely falling particles by hybrid immersed boundary–Lattice Boltzmann–discrete element method. Particulate Science and Technology, 2019.

[9] Yuan, H.-Z., et al., A momentum exchange-based immersed boundary-lattice Boltzmann method for simulating a flexible filament in an incompressible flow. Computers & Mathematics with Applications, 2014. **67**(5): p. 1039-1056.

[10] Gerivani, H. and M. Nazari, Proposing a lattice spring damper model for simulation of interaction between elastic/viscoelastic filaments and fluid flow in immersed boundary-lattice Boltzmann framework. Journal of Molecular Liquids, 2019. **296**: p. 111969.

[11] Moriche, M., O. Flores, and M. García-Villalba, *On the aerodynamic forces on heaving and pitching airfoils at low Reynolds number.* Journal of Fluid Mechanics, 2017. **828**: p. 395-423.

[12] Kang, S.K. and Y.A. Hassan, A comparative study of direct-forcing immersed boundary-lattice Boltzmann methods for stationary complex boundaries. International Journal for Numerical Methods in Fluids, 2011. **66**(9): p. 1132-1158.

[13] Guo, Z., C. Zheng, and B. Shi, *Discrete lattice effects on the forcing term in the lattice Boltzmann method.* Physical review E, 2002. **65**(4): p. 046308.

[14] Xiong, Q., et al., Nanofluid flow and heat transfer due to natural convection in a semi-circle/ellipse annulus using modified lattice Boltzmann method. International Journal of Numerical Methods for Heat & Fluid Flow, 2019.

[15] Afra, B., et al., Fluid-structure interaction for the flexible filament's propulsion hanging in the free stream. Journal of Molecular Liquids, 2021. **323**: p. 114941.

[16] Afra, B., et al., An immersed boundary-lattice Boltzmann method combined with a robust lattice spring model for solving flow–structure interaction problems. Applied Mathematical Modelling, 2018. **55**: p. 502-521.

[17] Zou, Q. and X. He, On pressure and velocity boundary conditions for the lattice Boltzmann BGK model. Physics of fluids, 1997. **9**(6): p. 1591-1598.

[18] Smits, A.J., *Undulatory and oscillatory swimming.* Journal of Fluid Mechanics, 2019. **874**.

[19] Lua, K.B., et al., *Effects of pitching phase angle and amplitude on a two-dimensional flapping wing in hovering mode.* Experiments in Fluids, 2015. **56**(2): p. 1-22.